Identification of cytokine-specific sensory neural signals by decoding murine vagus nerve activity

Theodoros P. Zanos[a,1], Harold A. Silverman[a,b,1], Todd Levy[a], Tea Tsaava[a,b], Emily Battinelli[a,b], Peter W. Lorraine[c], Jeffrey M. Ashe[c], Sangeeta S. Chavan[a,b], Kevin J. Tracey[a,b,2,3], and Chad E. Bouton[a,2,3]

[a]Center for Bioelectronic Medicine, Feinstein Institute for Medical Research, Manhasset, NY 11030; [b]Center for Biomedical Sciences, Feinstein Institute for Medical Research, Manhasset, NY 11030; and [c]General Electric Global Research US, Niskayuna, NY 12309

The nervous system maintains physiological homeostasis through reflex pathways that modulate organ function. This process begins when changes in the internal milieu (e.g., blood pressure, temperature, or pH) activate visceral sensory neurons that transmit action potentials along the vagus nerve to the brainstem. IL-1β and TNF, inflammatory cytokines produced by immune cells during infection and injury, and other inflammatory mediators have been implicated in activating sensory action potentials in the vagus nerve. However, it remains unclear whether neural responses encode cytokine-specific information. Here we develop methods to isolate and decode specific neural signals to discriminate between two different cytokines. Nerve impulses recorded from the vagus nerve of mice exposed to IL-1β and TNF were sorted into groups based on their shape and amplitude, and their respective firing rates were computed. This revealed sensory neural groups responding specifically to TNF and IL-1β in a dose-dependent manner. These cytokine-mediated responses were subsequently decoded using a Naive Bayes algorithm that discriminated between no exposure and exposures to IL-1β and TNF (mean successful identification rate 82.9 ± 17.8%, chance level 33%). Recordings obtained in IL-1 receptor-KO mice were devoid of IL-1β–related signals but retained their responses to TNF. Genetic ablation of TRPV1 neurons attenuated the vagus neural signals mediated by IL-1β, and distal lidocaine nerve block attenuated all vagus neural signals recorded. The results obtained in this study using the methodological framework suggest that cytokine-specific information is present in sensory neural signals within the vagus nerve.

cytokines | decoding | vagus nerve | inflammation | bioelectronic medicine

Evolutionary pressure, applied for millions of years, shaped the mammalian nervous system to control physiological homeostasis. Oxygenation, temperature, pH, blood pressure, hormones, mechanical factors, and metabolites activate sensory neurons to transmit action potentials to the spinal cord and brainstem. These sensory signals comprise the afferent arcs of basic reflex circuits that are activated by changes in the body's external and internal environment. This is the first step in modulating the outflow of motor neurons in the efferent arc of reflex circuits that control homeostasis. Reflex circuits regulate cellular function, metabolism, and blood flow in the visceral organs, thereby maintaining balanced output within a relatively narrow healthy and functional range. The vagus nerve, a paired structure arising in the brainstem and innervating the visceral organs, is comprised of 80,000–100,000 fibers in humans (1). It is the major sensory conduit for transmitting sensory signals from organs to the brain.

A large body of prior work defined reflex mechanisms controlling the cardiovascular, pulmonary, gastrointestinal, renal, hepatic, and endocrine systems, but only recently did advances in neuroscience and immunology reveal previously unrecognized mechanisms for the reflex control of inflammation (2, 3). Infection or injury activates immune cells to release cytokines, including TNF and IL-1β, and other factors that mediate inflammation. The production of these cytokines in the spleen is inhibited by neural signals that arise in the vagus nerve, travel in the splenic nerve, and culminate on lymphocytes that are activated to produce acetylcholine, a neurotransmitter molecule that interacts with its cognate receptor, α7 nAChR, expressed on macrophages and monocytes (3, 4). Acetylcholine-induced signal transduction increases intracellular calcium, decreases nuclear translocation of NFκB, stabilizes mitochondrial membranes, and inhibits inflammasome activity to reduce cytokine production (4). This prototypical neuronal reflex circuit is termed the "inflammatory reflex" (2, 5, 6). Targeting the inflammatory reflex using bioelectronic devices reduces cytokine production and inflammation in preclinical animal models of inflammatory diseases and in patients with rheumatoid arthritis and Crohn's disease (2, 6–10). The molecular mechanisms of the efferent arc are well defined, but considerably less is known about the afferent arc of the inflammatory reflex.

Early work revealed that afferent signals transmitted in the vagus nerve are required for the manifestation of a febrile response to IL-1β in rodents (11). Afferent vagus nerve signals are also implicated in mediating the development of sickness behavior in rodents, i.e., the syndrome of anorexia, behavioral withdrawal, and lethargy occurring when mammals are exposed to inflammatory challenges (12–14). Studies using vagus nerve-recording electrodes

Significance

Evolution conferred animals with molecular sensors that monitor cellular and organ function to detect changes in the environment. These activate sensory neural responses that drive the action of reflexes that maintain cellular and physiological homeostasis. Recent advances reveal that neural reflexes modulate the immune system, but it was previously unknown whether cytokine mediators of immunity mediate specific neural signals. Here we develop methods to isolate and decode specific neural signals recorded from the vagus nerve to discriminate between the cytokines IL-1β and TNF. This methodological waveform successfully detects and discriminates between specific cytokine exposures using neural signals.

in rats revealed that IL-1β administration given by intraportal injections increased the overall amplitude of the recorded activity of the vagus nerve (15, 16). Administration of endotoxin in healthy human subjects, experimental models, and clinical studies of rheumatoid arthritis and inflammatory bowel disease was associated with significant decreases in vagus nerve activity as measured by heart rate variability (17–22).

We have previously developed signal-processing tools to identify specific components of neural activity recorded using intracortical brain electrodes (23, 24). These recordings were comprised of the aggregate activity of neurons surrounding each intracortical electrode. Recorded signals from cerebral cortex were subjected to signal-processing techniques to assess responses to the subject's intended motor commands (23) or oculomotor modulations of visual processing (25, 26). These methods enabled the identification of functional neural circuits in response to specific behavior. We recently reported that administration of cytokines to mice induces sensory vagus nerve activity in a dose- and receptor-dependent manner (27). However, it was previously unknown whether it is possible to identify cytokine-specific neural signals encoded in the murine vagus nerve. Here, we developed a framework to isolate and decode the neural activity recorded on the surface of the vagus nerve in mice to identify groups of neurons firing in response to specific cytokines.

Results

Detection and Classification of Neural Activity. We recorded from the surface of the cervical vagus nerve in anesthetized mice using the CorTec Micro Cuff Sling bipolar electrodes (Fig. 1*A*). The raw recording acquired from the surface of the vagus nerve (Figs. 1*D* and 2*A*) included short-duration waveforms (<3 ms in width) that resembled neural impulses in their shape and rate (Fig. 1*D*). To confirm that these impulses are neural, lidocaine was applied to the nerve at the cervical level, distal to the electrode (*Methods*). As expected, we observed a significant decrease ($P < 0.001$, two-paired t test) in the rate of impulse activity of the nerve (Fig. 1*D*, *Upper*), with all impulses significantly attenuated or completely disappearing within 10 s after application of lidocaine (Fig. 1*D*, *Lower*). These experiments provided direct evidence that these impulses are the result of the propagating activity of specific neural pathways through single or multiple fibers discharging simultaneously.
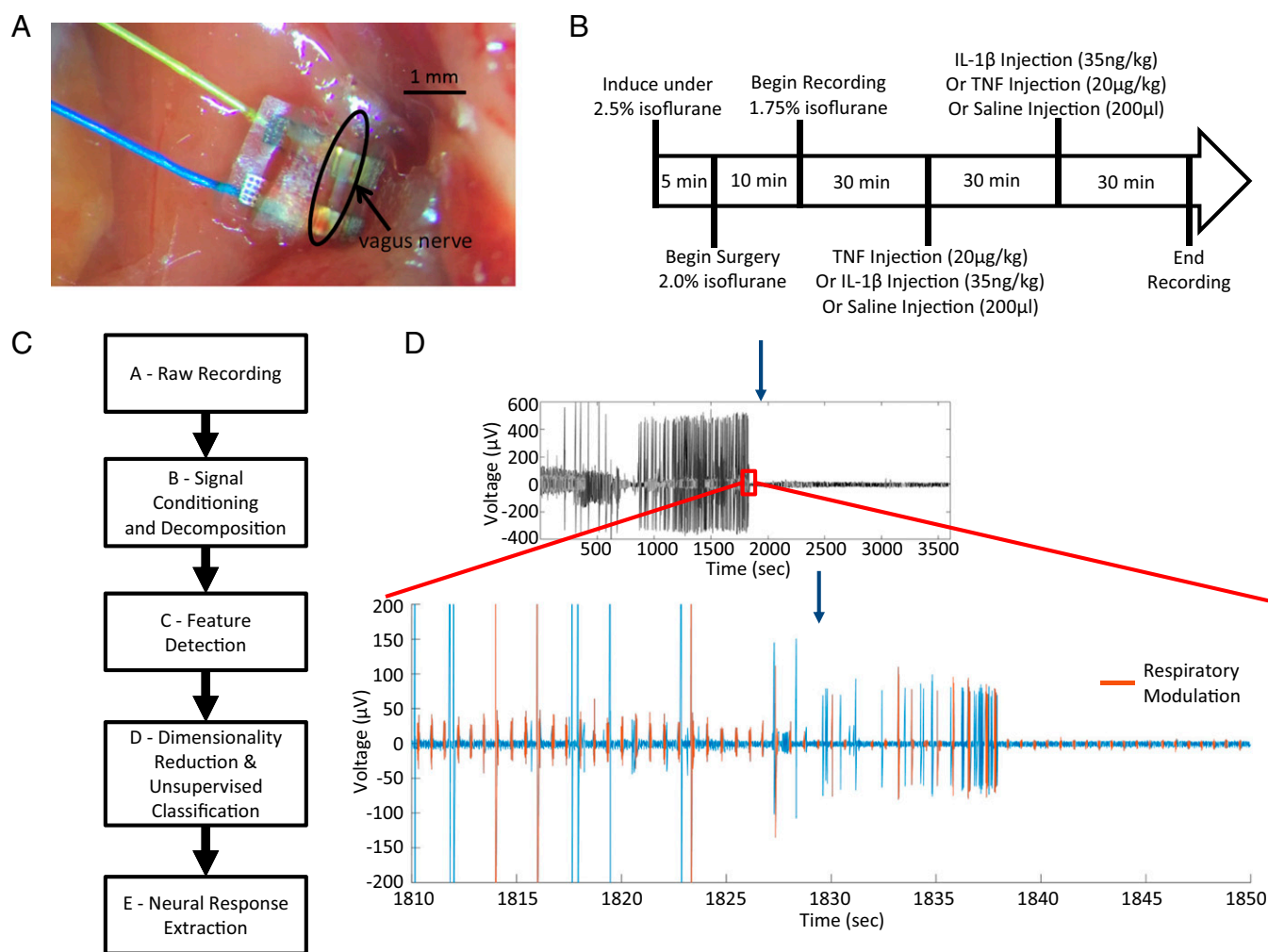

Fig. 1. Nerve recording interface, experimental design, preprocessing methodological framework, and raw surface recordings before and after lidocaine administration. (*A*) Photograph of the bipolar cuff electrode recording activity from the surface of the cervical vagus nerve of mice. (*B*) Schematic diagram of the cytokine-injection experiments, with TNF injected first and IL-1β second or IL-1β injected first and TNF injected second. (*C*) Schematic diagram of the preprocessing data-analysis methodological framework with all the steps carried out to extract neural responses. (*D*) Trace of raw surface recordings during experiments where lidocaine was dropped distally on the cervical vagus nerve (the time of lidocaine administration is indicated by the blue arrow). (*Upper*) The complete recording. (*Lower*) A zoomed-in portion of the recording around the time of the lidocaine drop, with respiratory modulations colored red.
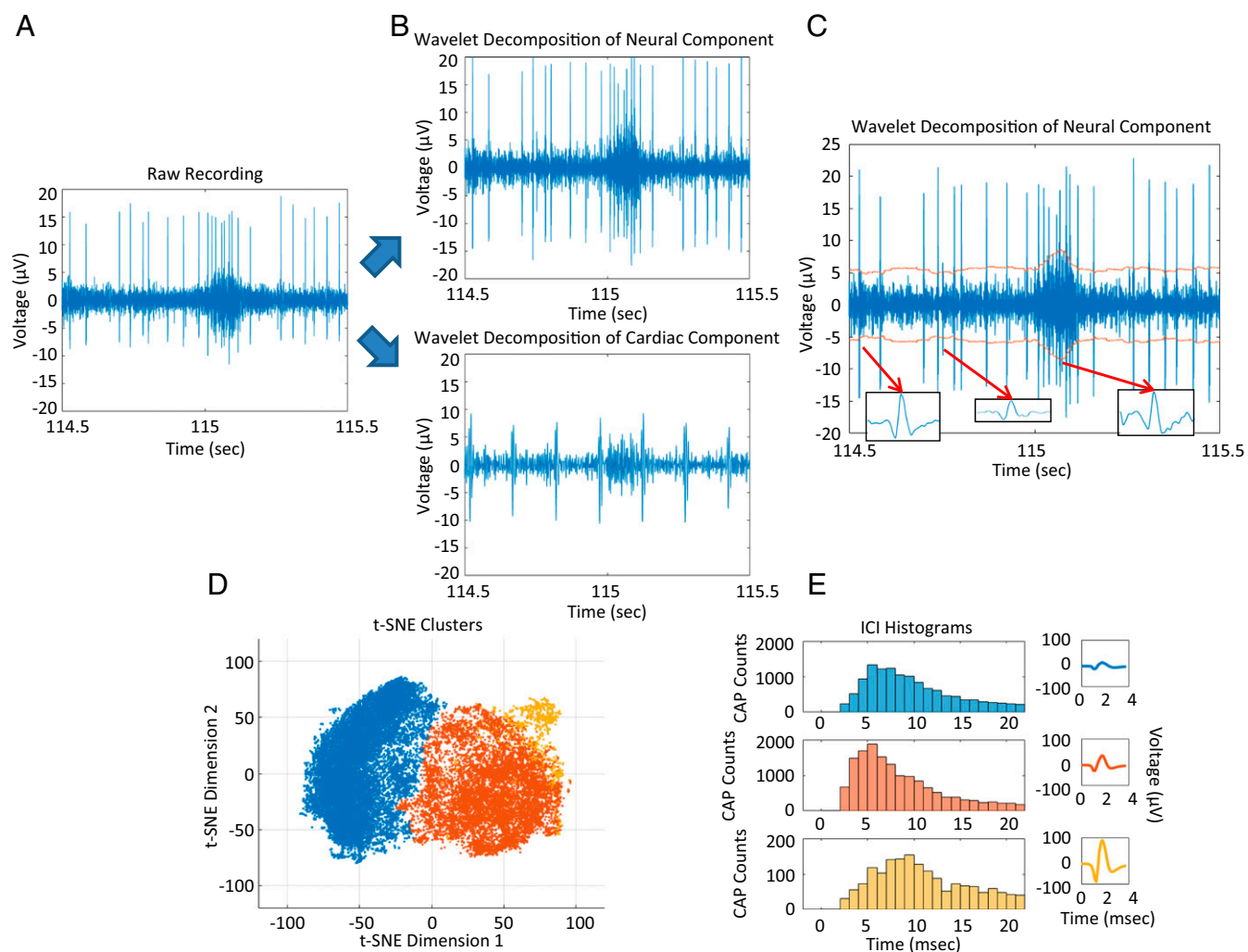
Fig. 2. Preprocessing framework. (*A*) The raw recorded signal. (*B*) Wavelet decomposition. (*C*) Adaptive thresholding. (*D*) Dimensionality reduction through t-SNE and clustering using the DBSCAN method. (*E*) Resulting CAP waveforms and inter-CAP interval (ICI) histograms.

In agreement with previous studies (27–29) these impulses are termed "compound action potentials" (CAPs).

The raw recording also included nonneural signals from cardiac, respiratory, and skeletomuscular activity. To separate the neural activity from nonneural signals, the raw data were filtered using wavelet decomposition that suppressed the lower-frequency cardiac signal (Fig. 2B). An adaptive thresholding method was used to identify individual impulses and account for respiratory-related modulations or changes in the nerve–electrode contact during the experiment. Applying these methods, we observed that the computed threshold follows respiratory modulations and identified neural impulses that occurred during and between these modulations (Fig. 2C).

Several factors (such as the number of fibers discharging and their size, propagation speed, and location relative to the recording electrode) are known to affect the shape and amplitude of the impulses detected in recordings (29, 30). Thus, sorting these waveforms by their shape and amplitude enables the examination of separate neural sensory groups. To this end, the proposed framework combined dimensionality reduction and unsupervised classification algorithms. Dimensionality reduction through the t-distributed stochastic neighbor embedding (t-SNE) method was employed to enable efficient visualization and clustering of the different groups of waveforms (Fig. 2D). Unsupervised classification through the density-based spatial clustering of applications

with noise (DBSCAN) algorithm determined the number of groups of waveforms and assigned each waveform (point in the dimensionality-reduced space) to a specific group (Fig. 2D). The amplitude and the shape of the waveforms within each clustered group differed significantly among groups (Fig. 2E). Moreover, neural groups are characterized by different firing-rate behaviors, as captured by the inter-impulse–interval histograms, which display the distribution of the intervals between two consecutive impulses. Finally, by computing the firing rates in CAPs per second using a 1-s binning window and a 30-s smoothing window, we derived the activity of the corresponding neural groups (Fig. 2E).

Administration of TNF and IL-1β to Mice Mediates Specific Vagus Nerve Firing Patterns. We and others have previously established that TNF, IL-1β, and other cytokines specifically activate calcium channels and action potentials in sensory neurons in the nodose ganglion and dorsal root ganglion (27, 31–36). To identify whether groups of neurons fire in response to TNF and IL-1β exposure, vagus nerve activity was recorded in wild-type mice ($n = 39$). We observed that specific groups of neurons changed their firing rates after TNF injection (Fig. 3A). Their response increased, plateaued, and persisted through the remainder of the recording. Subsequent IL-1β injection in the same animals did not affect the TNF-mediated response but instead triggered a response from another group of neurons (Fig. 3A). These results
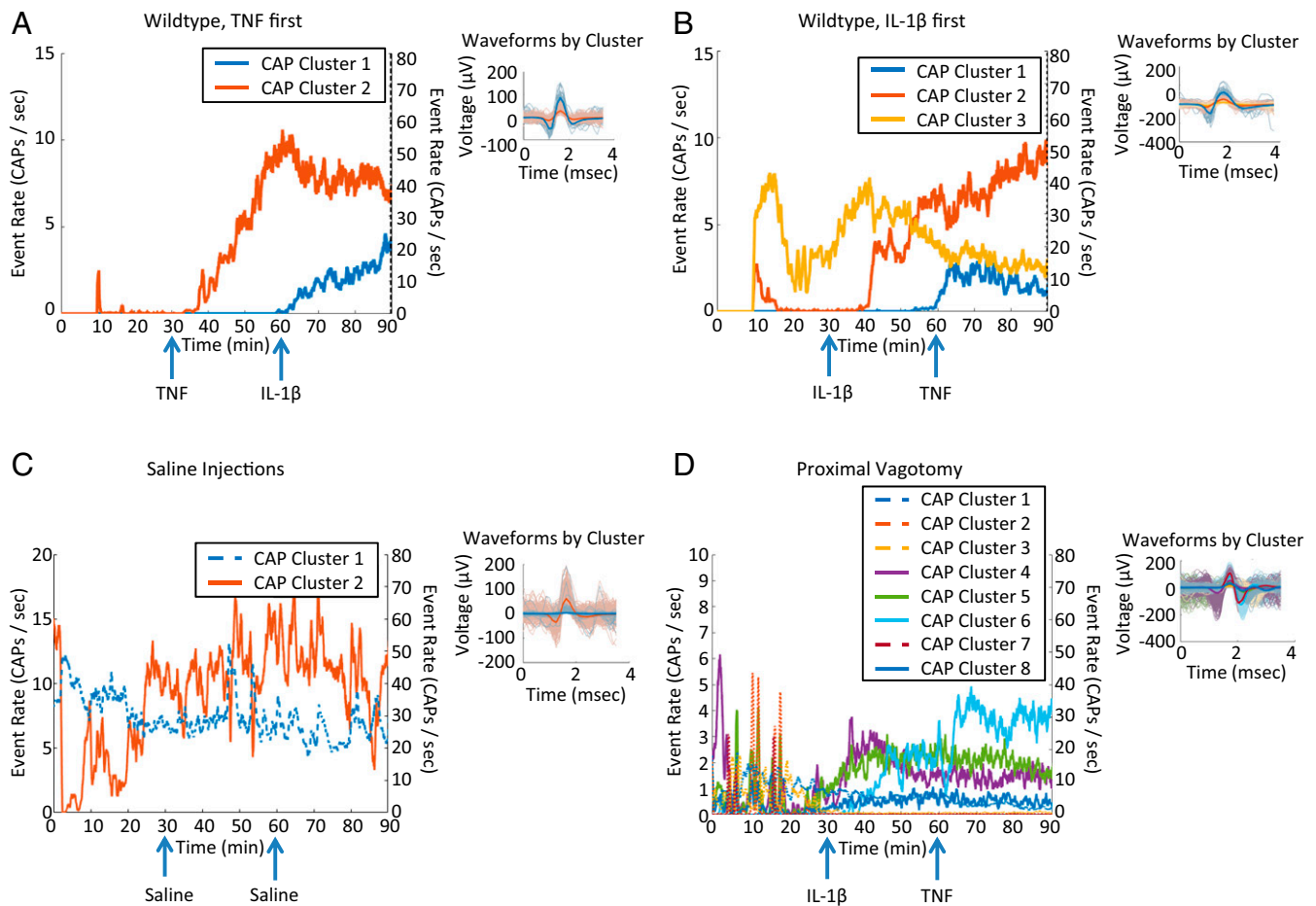
Fig. 3. Examples of neural responses to cytokines. Each colored trace represents the response rate against time of a different CAP. Solid lines correspond to lower-firing-rate CAPs (maximum of 15 CAPs/s), and dotted lines correspond to high-firing-rate CAPs (maximum of 80 CAPs/s). Right subpanel for all panels includes a subset of detected CAP waveforms and the median of each CAP group in thicker lines. (*A*) A vagus nerve response curve, along with the respective decoding accuracies, in a mouse injected first with 35 ng/kg IL-1β and then with 20 μg/kg TNF. (*B*) A vagus nerve response curve, along with the respective decoding accuracies, in a mouse injected first with 20 μg/kg TNF and then with 35 ng/kg IL-1β. (*C*) An example of neural responses to the saline injections control condition, where there is no discernible response to the injections. (*D*) A vagus nerve response curve in a mouse vagotomized proximally to the recording electrode and injected first with 35 ng/kg IL-1β and then with 20 μg/kg TNF.

were recapitulated in separate groups of animals that received IL-1β before the administration of TNF (Fig. 3*B*). These observations were tested across 39 mice by determining the number of responders to cytokine injections (Table 1). Mice were defined as "responders" when at least one CAP group deviated by 2 SDs from the peri-injection mean firing rate for at least one-third of the postinjection time period. We observed a response rate of 45% in animals receiving TNF first (9 of 20 mice) and a 73.7% response rate in the group receiving IL-1β first (14 of 19 mice). The cytokine-specific signals were not observed when mice received two injections of saline instead of TNF and IL-1β (*n* = 7) (Fig. 3*C*). These results were replicated in C57Black6 strain mice (Table 2 and *SI Appendix*, Fig. S2). To determine the afferent nature of these signals, we performed proximal vagotomy before TNF and IL-1β exposure and recorded vagus nerve activity in wild-type mice (*n* = 4). We observed both TNF- and IL-1β–related responses (Fig. 3*D*), with a response rate of 75% (three of four mice), similar to the intact vagus nerve recordings, providing evidence of their afferent, sensory nature.

Inspection of the recordings revealed that bursts of sensory neural group activity were synchronized with respiratory-related modulations in the vagus nerve recordings (Fig. 4*A*). Using a respiratory-modulation detector algorithm (*Methods*), we quantified the number of impulses that occur during respiratory modulation and compared

it with the total number of spikes for each CAP group. Twenty-three of the 29 detected groups that responded to cytokine injections were deemed respiration synchronized (over half of the impulses occurred during the respiratory modulation). To exclude the possibility that the observed firing-rate changes were mediated by similar changes in the respiratory-modulation rate or duration, we measured both rate

Table 1. Population results of the responders and decoding algorithm on all experiments

Group	Responders/total	Percent responders
Wild-type BALB\C, TNF 1st → IL-1β 2nd	9/20	45
Wild-type BALB\C, IL-1β 1st → TNF 2nd	14/19	73.7
Wild-type BALB\C, double saline	2/7	28.6
Wild-type C57Black6, IL-1β 1st → TNF 2nd	4/7	57.1
Proximal vagotomy, IL-1β 1st → TNF 2nd	3/4	75.0
TRPV1 cell-depleted IL-1β	1/6	16.6

Table 2. Performance of the decoding algorithm in successfully discriminating between the baseline, TNF, and IL-1β injection periods

Group	Baseline	TNF	IL-1β
Wild-type BALB\C, TNF 1st → IL-1β 2nd	93.5 ± 14.6	74.6 ± 18.5	88.7 ± 12.3
Wild-type BALB\C, IL-1β 1st → TNF 2nd	79.6 ± 28.6	69.8 ± 21.0	91.26 ± 11.9
Wild-type C57Black6, IL-1β 1st → TNF 2nd	83.9 ± 16.8	98.1 ± 1.7	85.7 ± 10.5
Proximal vagotomy, IL-1β 1st → TNF 2nd	83.1 ± 18.7	94.0 ± 4.7	57.6 ± 29.2
IL-1-R–KO, IL-1β 1st → TNF 2nd	60.9 ± 42.1	92.3 ± 5.9	17.5 ± 17.6

Data are shown as mean ± SD. Top row: TNF first-injection experiments; second row: IL-1β first-injection experiments in BALB\C mice; third row: IL-1β first-injection experiments in C57Black6 mice; fourth row: proximal vagotomy experiments; fifth row: IL-1R–KO experiments.

and duration across the length of all our recordings (Fig. 4B). The time courses of the respiratory-modulation rate and duration were consistent in all our recordings (Fig. 4B). These data indicate that changes in respiratory modulation or duration do not influence the firing rates of the sensory neural groups.

To confirm that the impulses co-occurring with the respiratory modulations were of neural origin and not due to artifacts from muscle activity or any other extraneural source, we examined whether firing rates attenuated after lidocaine administration. The respiratory-synchronized CAPs significantly attenuated or completely disappeared within 10 s after lidocaine administration (Fig. 1D, *Lower*). On the contrary, these recordings preserved small-amplitude modulations of the noise floor related to the respiratory cycle along with the cardiac artifacts. These results provided direct evidence that the respiratory-modulation–synchronized CAPs are of neural origin. We quantified these observations across all lidocaine experiments ($n = 6$ mice) by computing the normalized mean firing rate of all CAP groups before and after the lidocaine administration (300 s of activity in each window). This analysis revealed, as expected, a significant ($P < 0.001$, two-sample *t* test) drop in the firing rates of all CAP groups, respiratory synchronized or not (Fig. 4C). It should be noted that the residual activity after the lidocaine administration consists of attenuated impulse amplitudes and is mostly due to the adaptive nature of our impulse-detection threshold.

To automate the identification of cytokine-specific signals, we used a neural decoding algorithm based on the Naive Bayes method. Using the firing rates of different CAP groups as the input data, the algorithm attempted to identify the no-exposure (baseline) or exposure to a cytokine (TNF or IL-1β) conditions (Fig. 5A). To train this algorithm, neuronal responses were split into three groups of firing-rate values corresponding to the three different conditions (Fig. 5B), and the CAP groups responding to each injection were identified based on our responder rules, as outlined in *Methods* (Fig. 5C, *Left*). This decoding algorithm identified three different conditions in cases where either TNF or IL-1β was injected first (Figs. 5C, *Right* and 6 *A* and *B*) and performed poorly on the recording from an animal receiving only saline as the control (Fig. 6C). True positive fractions (percent correct) of all out-of-sample predictions (Table 2) were calculated to quantify the predictive accuracy of the decoding algorithm across all experiments. The success of decoding across all injections and conditions was 82.9 ± 17.8% correct; the probability of success of a random choice among the three classes is 33%.

Vagus Nerve Recordings of IL1 Receptor-KO Mice Contain Signals Specific to TNF and Not to IL-1β. The IL-1 receptor (IL-1R) has been implicated in the mediation of vagus nerve responses to IL-1β (11, 15, 16, 27). We next evaluated the changes in sensory neural group responses in IL-1R–KO mice. As shown in Fig. 7A, administration of IL-1β to IL-1R–KO mice did not induce vagus nerve enhancement. In contrast, TNF administration resulted in a significant change in the vagus nerve firing rate (Fig. 7A). Although the decoding algorithm failed to discriminate between

baseline and IL-1β, it correctly identified the TNF-mediated signal in IL-1R–KO mice (Fig. 7B), with a population success rate of 92.3% ± 5.9% (Table 2). These results demonstrate that the responses of sensory neural groups to IL-1β are mediated by the IL-1 receptor (IL-1R). The observed vagus nerve activity, mediated by TNF in the IL-1R–KO mice, gives direct evidence of cytokine-specific neural sensory groups.

TRPV1⁺ Neurons Are Required to Mediate Cytokine CAPs. TRPV1, a cation channel that is activated by capsaicin, heat, and acidic conditions as well as by other noxious stimuli, has been implicated in the transmission of pain signals and fever associated with inflammation (37–41). TRPV1 is expressed by a subset of sensory neurons whose cell bodies reside in dorsal root, trigeminal, and nodose/jugular ganglia (42, 43) and whose neuronal fiber types are mainly C and the slow-conducting Aδ fibers (44). TRPV1 is expressed in the subset of vagus afferent fibers and in brain nuclei
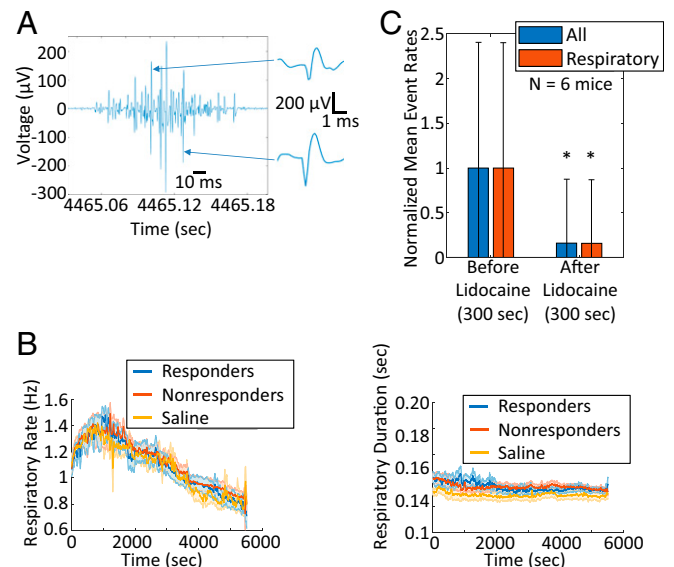

Fig. 4. CAP waveforms often occur during respiratory modulations of vagus nerve recordings and are silenced by lidocaine. (*A*) Representative example of the respiratory modulation apparent in most of our vagus nerve recordings, with several CAP waveforms occurring during this modulation (two CAP waveforms are plotted at the right of the panel). (*B*) Moving average respiratory-modulation rate (*Left*) and respiratory-modulation duration (*Right*), calculated throughout the time course of experiments, for three different experiment groups: responders to cytokine exposure (blue traces), nonresponders (red traces), and saline injections (yellow traces). The moving average of the SD is shown in the corresponding shaded colors. (*C*) Normalized mean firing rate and SD (error bars) of all CAP groups (blue) and all respiratory groups (red) across the lidocaine experiments ($n = 6$ mice), before and after the lidocaine drop. *Two-sample *t* test, $P < 0.001$.
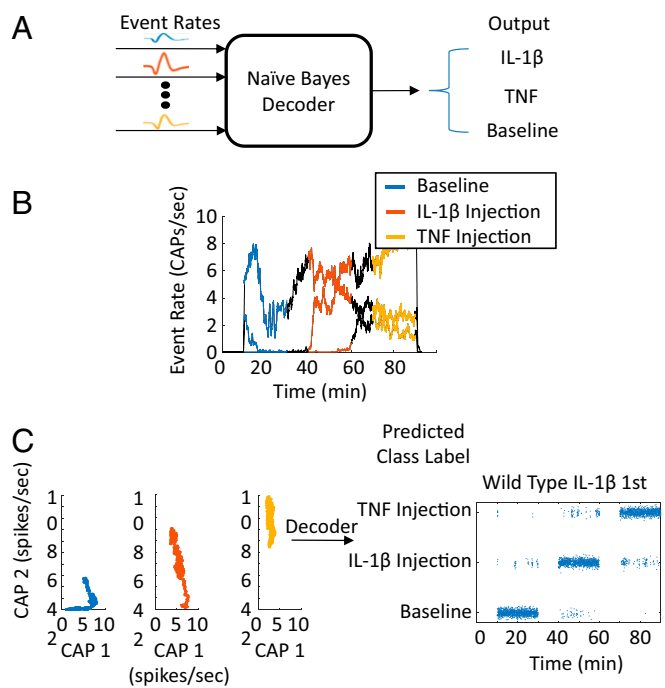
Zanos et al.

IMMUNOLOGY AND INFLAMMATION

ENGINEERING

Fig. 5. Decoding algorithm and illustrative example. (*A*) Schematic diagram of the decoder used to discriminate between no injection (baseline) and IL-1β or TNF injection. (*B* and *C*) Illustrative example of the transformation of the data from the time domain to the CAP response domain (*B*), where the decoder detects the two responding CAP clusters, thus grouping the response values into the three distinct classes, baseline or IL-1β or TNF injection, using threefold cross-validation (*C*, *Left*). (*C*, *Right*) The concatenated out-of-sample prediction of the algorithm from all the folds to validate our algorithm shows the result of the decoding and is indicative of its accuracy.

that receive vagus afferents and project to the nucleus of the solitary tract (45, 46). To determine whether cytokine-mediated responses propagate through TRPV1$^+$ fibers, we generated TRPV1-Cre/diphtheria toxin A (DTA) mice to selectively ablate TRPV1$^+$ cells. Vagus nerve activity was recorded in TRPV1-Cre/DTA mice in response to IL-1β administration, and no change in vagus nerve activity was observed following the administration of IL-1β (Fig. 7*C*). When looking at population results, we found that the responder rate of TRPV1-Cre/DTA mice to any of the cytokine injections was 16.6%, lower than the average responder rate of 58.9% in naive mice. These results indicate that IL-1β–specific sensory neural groups require TRPV1$^+$ fibers in the vagus nerve.

Administration of Different Doses of Cytokines Evokes Different Firing Patterns. We have previously recorded vagus nerve activity while administering different doses of TNF and IL-1β (27), demonstrating changes in the overall response rate of CAPs. To demonstrate that the same decoding framework can be used to identify exposure not only to different types of cytokines but also to different doses of a cytokine, we performed recordings injecting two different doses of the same cytokine (TNF or IL-1β). For TNF, the first injection was our previously used dose of 20 μg/kg, which was followed by a higher dose of 200 μg/kg; for IL-1β the first injection was our previously used dose of 35 ng/kg, which was followed by a higher dose of 350 ng/kg. As we demonstrated earlier, upon administration of TNF (20 μg/kg) or IL-1β (35 ng/kg), specific groups of neurons change their firing rate (Fig. 8 *A* and *B*). Subsequent injection of IL-1β induced a response from the same sensory group (yellow trace in Fig. 8*A*) as the first injection, with an increased firing rate and faster response time. The higher dose of IL-1β also evokes a delayed response from a different CAP group

(red trace in Fig. 8*A*). Subsequent injection of TNF induces a similar response pattern (dark red trace in Fig. 8*B*). These observations were tested across 13 mice by determining the number of responders to double-dose injections (Table 3). Using the firing rates of these CAP groups as the input data to our decoding algorithm, we were able to discriminate between low and high doses of each cytokine (Fig. 8 *C* and *D*). The success rates of the double IL-1β are shown in Table 4.

Discussion

Our results demonstrate that afferent signals in the vagus nerve encode cytokine-specific information. Using our signal-processing methods, we show that the electrical signals recorded on the cervical vagus nerve can be decoded to discriminate between cytokine-specific signals. Discrimination of the electrical activity transmitted through peripheral nerves using a preprocessing and decoding framework provides insights at the interface between the nervous and immune system.

Afferent signaling is generated through signaling cascades emanating from receptors. Binding of cytokines such as IL-1β and TNF to their respective cognate receptors on a subset of afferent fibers results in the activation of these sensory signals in the vagus nerve (27, 47). In this study, we demonstrate that TNF and IL-1β exposure manifests as unique signaling patterns which persist throughout the recording and are not modified by subsequent
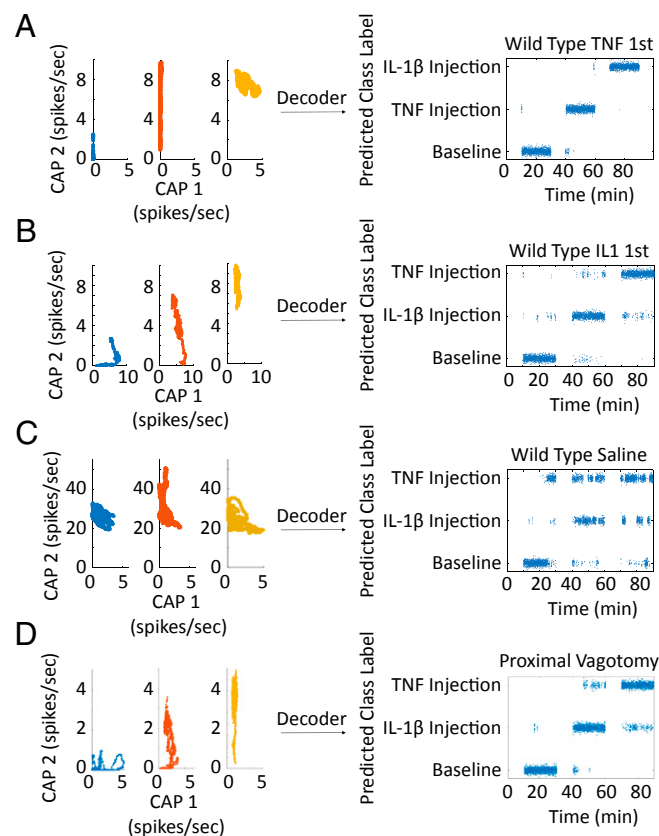
Fig. 6. Examples of decoder input and output. (*A* and *B*) Indicative examples of the 20 μg/kg TNF first injection/35 ng/kg IL-1β second injection experiments (*A*) and 35 ng/kg IL-1β first injection/20 μg/kg TNF second injection experiments (*B*). It is clear that the different injections elicit different responses and thus are successfully decoded. (*C*) An indicative example of the saline control experiments in which the responses are overlapping, leading to evidently poor decoding performance. (*D*) An indicative example of the experiment in which vagotomy was performed proximal to the recording electrode. It is clear that the different injections elicit different responses and thus are successfully decoded.

Fig. 7. Neural responses are receptor and fiber type specific. Shown are indicative examples of neural responses to different injections 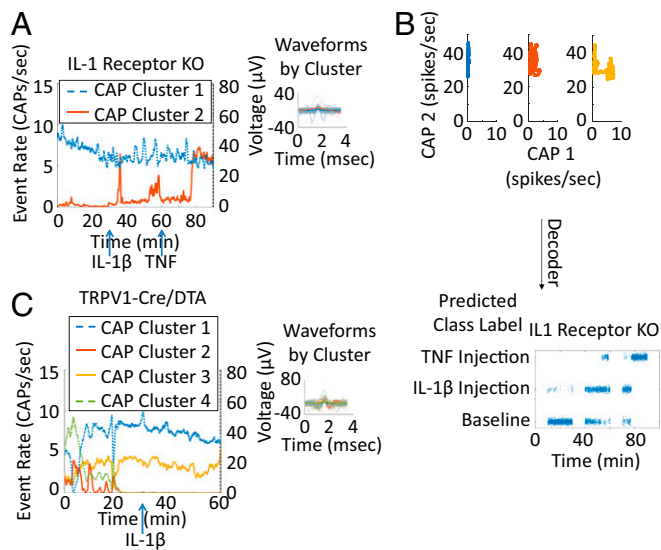and control experiments. Each colored trace represents the response rate against time of a different CAP. Solid lines correspond to lower-firing-rate CAPs (maximum of 15 CAPs/s). Dotted lines correspond to high-firing-rate CAPs (maximum of 80 CAPs/s). (*A*) An example of neural responses from an IL-1βR–KO mouse injected first with 35 ng/kg IL-1β and second with 20 μg/kg TNF. There is no significant IL-1β response (the response does not cross the responder thresholds), and there is a clear and significant response to the subsequent TNF response. (*B*) An indicative example of decoder input and output in the IL-1R–KO control experiment in which the baseline and IL-1β–injection responses overlap but the TNF injection is separated and successfully decoded. (*C*) An example of a TRPV1-Cre/DTA mouse injected with 35 ng/kg IL-1β with no significant postinjection response. Right subpanels for *A* and *C* include a subset of detected CAP waveforms and the median of each CAP group in thicker lines.

cytokine injections. These signals are identified as the firing rates of specific CAP waveforms that could emanate from the activation of these cytokine-specific receptors. The identification of specific CAP groups correlating with the administration of TNF suggests that a subset of vagus nerve fibers is signaling in response to individual cytokine challenge. Administration of larger doses of both cytokines evokes higher firing rates of the CAP waveforms that initially responded as well as the recruitment of additional nerve fibers manifested as a separate response of different CAP waveforms. These signals could originate at the receptor level, which, as previous studies have indicated, may be located directly on sensory neurons (27, 33). Additional to this direct effect, these sensory signals could also be attributed to indirect effects, as indicated by the presence of both fast (up to several seconds) and delayed (up to several minutes) neural responses. Injection of IL-1β or TNF leads to immune activation, i.e., the release of other cytokines, ATP, glutamate, or other neurotransmitters (2, 3, 41), that could be sensed by the vagal afferents. An important point is that TNF and IL-1β receptors have been previously reported to colocalize but not necessarily overlap completely (27).

IL-1β signaling generates action potentials in sensory neurons including the nodose ganglion, dorsal root ganglion, and trigeminal nerves (48–51). Previous studies have shown that TNF and IL-1β increase the excitability and sensitivity of nociceptor neurons (27, 31, 34, 35). TRPV1 is a ligand-gated nonselective calcium permeable ion channel. It integrates multiple physical and chemical stimuli, including vanilloid compounds, low pH, and noxious heat (37, 52, 53). A subset of vagus sensory afferents, including unmyelinated C fibers and myelinated Aδ fibers, express TRPV1 (54, 55). Utilization of the genetic cell-depletion model

for TRPV1+ cells allows us to establish not only that the IL-1β signal is exclusively sensory in its nature but also that it propagates through the specific TRPV1+ vagal fibers. TRPV1-Cre/DTA mice do not have detectable signal changes in vagus nerve activity in response to IL-1β administration. Taken together, the data presented here model the afferent signaling of the vagus nerve beginning with a specific receptor (IL-1 or TNF receptor) and with IL-1β activating a subset of vagus nerve fibers which are TRPV1+.

Extraneural peripheral nerve recordings, such as the ones used in this study, have specific benefits and drawbacks compared with intraneural recordings. While intraneural recordings with penetrating electrodes provide a higher signal-to-noise ratio (SNR) and spatial specificity, extraneural nerve cuff recordings minimize the risk of damage (56) and have been safely implanted chronically in humans (57, 58). However, current nerve-surface recordings suffer from relatively low spatial specificity. While novel nerve electrodes with multiple contacts are aimed at improving the quality and information content of the recordings (59–62), parallel attempts utilizing signal-processing and data-analysis methods have shown promise in achieving similar goals (63, 64). Until now, however, linking such signals with functional sensory stimuli has been applied mainly by using muscle proprioceptive or somatosensory stimuli in larger nerves (for example sciatic and median nerves). In the current study, the proposed neural recording data-analysis framework paired with cytokine injections reveals specific functional pathways activated by cytokine challenges. As previously demonstrated by detailed biophysical models (29), differences in the size and spatial location of activated groups of fibers or fascicles can produce CAP waveforms, picked up at the surface of the nerve, that differ in their amplitude and shape. Thus, the strategy of clustering detected CAPs to different groups based on their waveform properties can potentially separate signals mirroring the activation of different groups of fibers
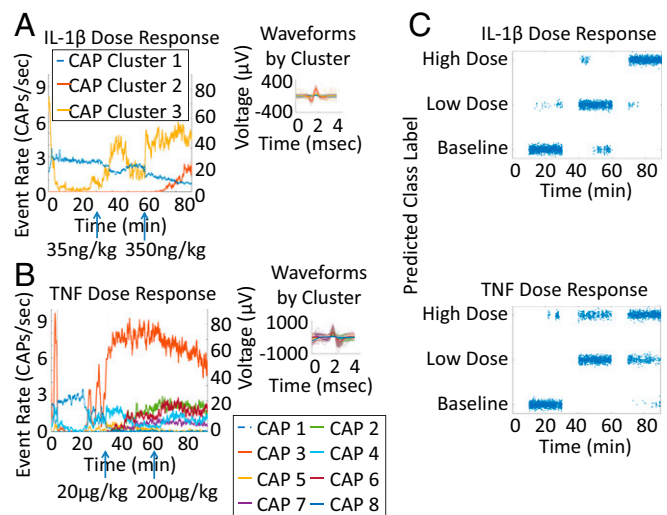

Fig. 8. Different doses of cytokines evoke different patterns. Indicative examples of neural responses to different doses of a cytokine. Each colored trace represents the response rate against time of a different CAP. Solid lines correspond to lower-firing-rate CAPs (maximum of 15 CAPs/s). Dotted lines correspond to high-firing-rate CAPs (maximum of 80 CAPs/s). (*A, Left*) An example of neural responses from double-dose IL-1β injections, where we first injected 35 ng/kg IL-1β and then injected 350 ng/kg IL-1β, showing a clear and significant response to both injections. (*B*) An example of neural responses from double-dose TNF injections, where we first injected 20 μg/kg TNF and then injected 200 μg/kg TNF, showing responses to both exposures. (*C*) Decoder output of the double-dose IL-1β injections (*Upper*) and TNF injections (*Lower*). In both cases, the two consecutive doses are successfully decoded. Right subpanels for *A* and *B* include a subset of detected CAP waveforms and the median of each CAP group in thicker lines.

Zanos et al.

IMMUNOLOGY AND INFLAMMATION

ENGINEERING

www.manaraa.com

Table 3. Population results of the responders for the double-dose experiments

Group	Responders/total	% responders
Wild type, IL-1β 1st dose → IL-1β 2nd dose	5/7	71.4
Wild type, TNF 1st dose → TNF 2nd dose	4/6	66.7

or fascicles. Combining temporal information from the cytokine challenges with the decomposed CAP waveforms can be further expanded by the use of multielectrode neural interfaces, enabling a deeper understanding of the types of fibers involved in the decoded signaling of the inflammatory reflex.

The majority of the recordings in this study featured co-occurring respiratory modulations, an interesting feature that prompted further experiments and analysis that confirmed the neural nature of the CAP waveforms (through the lidocaine experiments). While micromotion of the cuff electrode relative to the vagus nerve due to respiratory movements could contribute to these modulations, the nerve-block experiments showed that it does not account for a significant percentage of the modulation. One reason for this co-occurrence would be that these cytokine-related neural impulses could be occurring throughout the experiment but are compounded, and thus amplified, by larger-amplitude breathing-related sensory neural signaling (65). Another possibility would be that respiratory-related rapidly adapting stretch receptors, along with C fibers, are also encoding for irritants and cytokines, perhaps mediating cough responses (66–68). However, further experiments of concurrent vagus nerve recordings and genetic control of vagal sensory neuron subtypes are needed to test these hypotheses. Finally, it is possible that these sensory neural responses could also help mediate mood or behavioral responses by signaling cytokine changes to emotional and cognitive centers through the gut–brain axis (2, 3, 69, 70). While the focus of this study is on the afferent arm of the inflammatory reflex, similar approaches could be used to resolve the encoding of other biomarkers related to metabolic, cardiac, or pulmonary functions.

Methods

Electrophysiological Recordings and Experimental Design.

Animals. All experimental protocols were approved by the Institutional Animal Care and Use Committee at the Feinstein Institute for Medical Research, Northwell Health, which follows the NIH guidelines for ethical treatment of animals. Male BALB/c, C57 Black 6, and IL-1R–KO mice (strain B6.129S7-Il1r1tm1Imx/J) were purchased from Charles River or Jackson Laboratory and were used between 8 and 16 wk of age. TRPV1-Cre/DTA or TRPV1 cell-depleted mice were bred at the Feinstein Institute for Medical Research and were used between 8 and 16 wk of age. (Homozygous TRPV1-Cre males were bred to homozygous lox-DTA females.) Mice were housed under a 12-h reverse-day light cycle and had access to food and water ad libitum. Food was withheld for 3–4 h before nerve recording; during this time the animals continued to have access to water.

Surgical isolation of the cervical vagus nerve. The surgical and recording methods have been previously described (71). Mice were induced with general anesthesia using isoflurane at 2.5% in 100% oxygen at a flow rate of 1 L/min for 5 min. Mice were then placed in the supine position and maintained at 2.0% isoflurane during surgery. The core body temperature was monitored with a rectal probe and was maintained around 37 °C with a heating pad and heat lamp. To expose the cervical vagus nerve, the neck area was shaved and cleaned with povidone iodine, and a midline cervical incision was made from the level of larynx to the sternum. The submaxillary salivary glands were exposed by blunt dissection and separated through the midline fascial plane to expose the trachea. The bundle is readily identified by the pulsation of the artery. The cervical vagus nerve was delicately separated from the artery and desheathed by gently removing the thin connective tissue surrounding the nerve under magnification. A ground electrode was inserted between the right salivary gland and the skin. The nerve was then placed on a bipolar sling platinum-iridium cuff electrode (CorTec) that was submerged briefly in saline

before nerve placement within the cuff (Fig. 1A). The surgical area was covered with Parafilm to ensure that the nerve and surgical area did not desiccate (27).

Cervical vagus nerve vagotomy. The cervical vagus nerve was isolated as described earlier. Before vagotomy, a silk suture was secured to the vagus nerve with a single knot. A surgical cut of the vagus nerve was performed proximal to the recording electrode and suture using the brain as the point of reference.

Recording procedure. The electrophysiological signals for BALB/c, IL1R-KO, and TRPV1-Cre/DTA mice were digitized from the cervical vagus nerve using a Plexon data-acquisition system (OmniPlex; Plexon, Inc.) (27). Isoflurane was maintained at 1.75% for BALB/c mice and at 1.25% for C57 Black 6, IL1R-KO, and TRPV1-Cre/DTA mice throughout the recording. Thirty minutes of baseline activity were recorded followed by an i.p. injection of either TNF (20 μg/kg) or IL-1β (35 ng/kg) (Fig. 1B). Vagus nerve activity was then acquired for 30 min, followed by a second injection of the alternate cytokine (TNF or IL-1β). Another 30 min of activity was acquired after the second injection. Control animals were injected with saline following the design described above (Fig. 1B). Increasing-dose injections were done with the same experimental design; however both injections were of the same cytokine, with a 10×-higher dose used for the second injection (200 μg/kg TNF or 350 ng/kg IL-1β). For the lidocaine experiments, 30 min of baseline activity were recorded. Ten microliters of saline were applied distally on the nerve at 10 or 20 min into baseline recording to establish that there was no shunting due to the drop of liquid distally to the electrodes; in all six experiments the activity was not affected by the saline drop. Approximately 30 min into each recording, a 10-μL drop of lidocaine (200 mg/mL concentration) was applied distally on the nerve, and 30 more minutes of recordings were acquired. To make sure we were not blocking muscle activity, a small patch of Parafilm was inserted below the recording electrode and above all other tissue, limiting the drop of lidocaine to the nerve.

Data Analysis. All recordings and the Matlab code for analysis and algorithms are available for download at public.feinsteininstitute.org/cbem/PNAS%20Submission/. The signal-processing framework conditions the raw vagal recordings and extracts information from them so that we can decode the neural signals to injection-induced changes in the levels of the inflammatory cytokines IL-1β and TNF. This framework consists of signal decomposition to cardiac and neural components, detection of CAP waveforms, dimensionality reduction of the CAP waveforms, unsupervised CAP clustering, and neural response extraction (Fig. 1C). Finally, a decoding classification algorithm based on the extracted neural responses predicts injection states (no injection or IL-1β or TNF injection).

Signal Decomposition. Raw surface vagal recordings are an aggregate of nerve activity and various other signal sources, physiological and nonphysiological (Fig. 2A). Apart from instrumentation-related sources of interference, in nerve recordings there are also biological sources of interference, such as cardiac events. We exploit the duration of the cardiac events due to cardiac action potentials to filter them from the data. Wavelet decomposition using a Daubechies 3 (Db3) wavelet at a 5-ms scale was used to isolate cardiac artifacts, while wavelet decomposition using a Db3 wavelet at a 1-ms scale was used to emphasize CAPs (Fig. 2B).

Detection of Action Potentials. Vagus nerve recordings acquired at the cervical level typically include a respiratory modulation of the signal envelop (67, 72), causing the statistics associated with the signals to be cyclostationary. For this reason, an adaptive CAP threshold was preferred from a constant-valued threshold, and a smallest of constant false-alarm rate (SO CFAR) filter (73) was used to determine the threshold that rides on the respiratory modulation. CFAR filters use a sliding window to estimate the background statistics of a signal so that a threshold that maintains a constant false-alarm rate on average can be applied on a per-window basis. This allows the threshold to accommodate relatively abrupt transitions in the background statistics. The parameters of the threshold that was used across all subjects were the window

Table 4. Population results of the decoding algorithm accuracy on the double-dose experiments

Group	Baseline	Low dose	High dose
Wild type, IL-1β low dose → IL-1β high dose	87.5 ± 18.3	74.6 ± 15.8	91.5 ± 10.5
Wild type, TNF low dose → TNF high dose	91.3 ± 8.6	76.2 ± 22.8	67.1 ± 31.9

Data are shown as mean ± SD.

www.manaraa.com

duration (188 ms on each side), the guard cell duration (13 ms on each side), and the threshold level (3 SDs from the mean). These parameters were heuristically chosen based on empirical results that were dependent on the period and duty cycle of the respiratory modulation, which was similar for all subjects. We applied this adaptive threshold to the decomposed neural signal (from the 1-ms db3 wavelet decomposition) and identified CAP instances (Fig. 2C).

The cardiac-enhanced signal was also thresholded using a constant threshold to detect the times at which cardiac events occurred. Detected CAPs that coincided with detected cardiac events were discarded. A refractory period of 1 ms was also applied to prevent multiple threshold crossings right after the detection of a CAP.

Dimensionality Reduction. Once a set of CAP waveforms had been detected through thresholding, groups of CAP waveforms were identified based on their shape and amplitude through nonlinear dimensionality reduction followed by unsupervised clustering. We hypothesized that these distinct groups of CAPs correspond to individual or groups of fibers within the vagus nerve that are firing to create the different shape and amplitude CAP waveforms picked up at the surface of the nerve.

The t-SNE method was used to perform nonlinear dimensionality reduction. t-SNE converts the distances between the data points to Gaussian and t-distributed joint probabilities in the high- and low-dimensional spaces, respectively, and it subsequently attempts to minimize the Kullback–Leibler divergence between the joint distributions as a way to preserve similarity between the data points in the original and reduced spaces (74). The dimensionality of the original space, typically 120 samples corresponding to the number of samples in a detected CAP waveform, is reduced to two dimensions.

Since t-SNE has $O(N\log N)$ complexity and uses $O(N^2)$ memory and because in a typical 90-min vagal recording it is common to detect more than 100,000 CAPs, the kernel t-SNE extension (75) was employed to reduce the data points on which the dimensionality reduction is performed. The kernel t-SNE extension uses kernels to approximate the local curvature of the original manifold and provides a way to predict where new points would map in the reduced dimensional space, as long as appropriate kernel parameters are chosen. Five thousand CAP waveforms were uniformly sampled throughout the entire recording; t-SNE was performed on this subset of detected waveforms, and kernel t-SNE was subsequently used. The method formed clusters in the data when there were distinct CAP waveform shapes and amplitudes (Fig. 2D).

Unsupervised Classification. Once dimensionality reduction was performed, the DBSCAN clustering algorithm (76) was used as an unsupervised method that identified and separated distinct clusters. DBSCAN was applied only to the original t-SNE data points, since it also scales $O(N^2)$ in memory. The two parameters of the method were chosen heuristically: The density parameters were set to 5.9 and 10, and the minimum number of points required to form a cluster was set to 30. K-nearest neighbors (KNN) with $K = 5$ was used to perform semisupervised classification for the remainder of the CAP waveforms that were mapped using kernel t-SNE.

Neural Response Extraction. Each cluster of CAP waveforms can be inspected visually by the average waveform and the distribution of inter-CAP intervals (Fig. 2D) to reveal artifacts (waveform widths of more than 3 ms, abnormal shapes or discontinuities in the waveform, abnormal peaks in the inter-CAP intervals), which were discarded from further analysis.

As mentioned earlier, the main hypothesis for sorting CAP waveforms into different groups (clusters) is that different CAP waveform shapes and amplitudes represent the activity of different groups of nerve fibers. To derive the firing rates of these groups, event rates were computed by binning the detected CAP waveforms of each group in 1-s windows, resulting in an event-rate signal measured in CAPs per second (Fig. 3). The event rates of the different CAP groups contain features that could be correlated with the cytokine injections and could be used for neural decoding of the different states.

Determining Responsive Sensory Neural Groups. Naturally, not all sensory neural groups are expected to contain information related to changes in cytokines. While consistent changes in the event rates of specific CAP clusters directly after a cytokine injection were observed, many CAP clusters had event

rates that fluctuated in ways unrelated to the experimental challenges. To reduce model complexity while increasing efficiency, a method to determine responders—CAP clusters that exhibited significant event-rate modulations due to cytokine injection—was developed. By measuring the SD, σ, of the baseline activity (between 10 and 30 min from the initiation of recording) and the mean firing rate, μ, for 4 min before an injection, a threshold was set at $\mu \pm k*\max(\sigma_{min}, \sigma)$ and was applied to the signal corresponding to 10–30 min after each injection. The parameter k is a constant, and σ_{min} is a lower bound on the measured SD, so that the response in cases of very-low-amplitude baseline SDs does not become sensitive to insignificant changes in the firing rate. Since we are interested in sustained responses, for a CAP waveform cluster to be labeled as a responder, the firing rate at the specified postinjection time has to be above the upper bound $[\mu + k*\max(\sigma_{min}, \sigma)]$ or below the lower bound $[\mu - k*\max(\sigma_{min}, \sigma)]$ for at least one-third of the postinjection duration (7 min).

Based on these criteria, two of the seven subjects that were given saline injections appeared to elicit a vagal response. We thus maximized the number of cytokine responders constrained to a false-alarm rate of two saline responders by performing a grid search over k, σ_{min}, and the event-rate smoothing parameter, s, yielding the values $k = 2.5$, $\sigma_{min} = 2$, and $s = 5$; 23 of 39 mice were responders to at least one of the two cytokine injections.

Respiratory-Modulation Detector. Since a large number of the CAP impulses detected occur mainly during respiratory bursts, we needed to robustly detect the respiratory-related modulation in our signal and quantify the exact amount of impulses that occur during its duration. Thus, a respiratory-modulation detector was developed that was able to measure the time of occurrence and the duration of these modulations. A rolling SD of the recordings was computed. The peaks of the rolling SD signal constrained by the minimum peak distance, minimum peak prominence, minimum peak width, and maximum peak width were found. The minimum peak width constraint complemented the outlier filtering, and the minimum peak width was set slightly larger than the rolling window duration. The maximum peak width constraint was used to avoid detecting unrealistically long bursts that may occur in low-SNR conditions. The minimum peak prominence constraint was used for the sensitivity/specificity trade-off: Too low a value would detect too many false respiratory bursts, and too high a value would miss many real respiratory bursts. The minimum peak distance was a constraint that sets a lower bound the respiratory rate.

After detecting the respiratory intervals and the locations of the CAPs, we counted the CAPs that occurred within the respiratory intervals and computed their percentage relative to their total number throughout the recording. Since the measured rate of these respiratory modulations was roughly 1/s, and their duration never exceeded 250 ms, CAP groups with more than half of their impulses occurring during this modulation were considered respiration synchronized.

Neural Decoding. To assess whether neural responses to cytokine injections can be used to determine the state of the subject, a Gaussian Naive Bayes classifier was trained using only responsive CAPs. To avoid overfitting, threefold cross-validations were repeated 30 times as a form of ensemble averaging. The confusion matrix, a table that relates the actual class to the predicted class, was formed by summing the posterior probabilities of the class that has the maximum posterior. In this application, the three classes, corresponding to the different states of the subject, were baseline, IL-1β injection, and TNF injection. These classes corresponded to activity from 10 min after an injection or the start of the recording until the next injection, which occurred 30 min following the initial injection. The first 10 min of the postinjection recordings were not used to avoid training on transient responses, which usually occurred during that specific period. We quantified the predictive ability of the decoder by estimating the percentage of correct classifications on out-of-sample data. The percent correct of the decoder was determined as the true positives of the classifier weighted by the confidence of the prediction.

1. Hoffman HH, Schnitzlein HN (1961) The numbers of nerve fibers in the vagus nerve of man. *Anat Rec* 139:429–435.
2. Chavan SS, Tracey KJ (2017) Essential neuroscience in immunology. *J Immunol* 198:3389–3397.
3. Pavlov VA, Tracey KJ (2017) Neural regulation of immunity: Molecular mechanisms and clinical translation. *Nat Neurosci* 20:156–166.
4. Olofsson PS, Rosas-Ballina M, Levine YA, Tracey KJ (2012) Rethinking inflammation: Neural circuits in the regulation of immunity. *Immunol Rev* 248:188–204.
5. Tracey KJ (2002) The inflammatory reflex. *Nature* 420:853–859.
6. Andersson U, Tracey KJ (2012) Reflex principles of immunological homeostasis. *Annu Rev Immunol* 30:313–335.
7. Huston JM, Tracey KJ (2011) The pulse of inflammation: Heart rate variability, the cholinergic anti-inflammatory pathway and implications for therapy. *J Intern Med* 269:45–53.
8. Levine YA, et al. (2014) Neurostimulation of the cholinergic anti-inflammatory pathway ameliorates disease in rat collagen-induced arthritis. *PLoS One* 9:e104530.

Zanos et al.

www.manaraa.com

IMMUNOLOGY AND INFLAMMATION

ENGINEERING

9. Koopman FA, et al. (2016) Vagus nerve stimulation inhibits cytokine production and attenuates disease severity in rheumatoid arthritis. *Proc Natl Acad Sci USA* 113: 8284–8289.

10. Bonaz B, et al. (2016) Chronic vagus nerve stimulation in Crohn's disease: A 6-month follow-up pilot study. *Neurogastroenterol Motil* 28:948–953.

11. Watkins LR, et al. (1995) Blockade of interleukin-1 induced hyperthermia by subdiaphragmatic vagotomy: Evidence for vagal mediation of immune-brain communication. *Neurosci Lett* 183:27–31.

12. Dantzer R (2009) Cytokine, sickness behavior, and depression. *Immunol Allergy Clin North Am* 29:247–264.

13. Pavlov VA, Tracey KJ (2012) The vagus nerve and the inflammatory reflex–linking immunity and metabolism. *Nat Rev Endocrinol* 8:743–754.

14. Goehler LE, et al. (2000) Vagal immune-to-brain communication: A visceral chemosensory pathway. *Auton Neurosci* 85:49–59.

15. Niijima A (1996) The afferent discharges from sensors for interleukin 1 beta in the hepatoportal system in the anesthetized rat. *J Auton Nerv Syst* 61:287–291.

16. Niijima A, Hori T, Katafuchi T, Ichijo T (1995) The effect of interleukin-1 beta on the efferent activity of the vagus nerve to the thymus. *J Auton Nerv Syst* 54:137–144.

17. Jan BU, et al. (2009) Influence of acute epinephrine infusion on endotoxin-induced parameters of heart rate variability: A randomized controlled trial. *Ann Surg* 249: 750–756.

18. Ziegler D, et al. (2015) Differential patterns and determinants of cardiac autonomic nerve dysfunction during endotoxemia and oral fat load in humans. *PLoS One* 10: e0124242.

19. Goldstein RS, et al. (2007) Cholinergic anti-inflammatory pathway activity and high mobility group box-1 (HMGB1) serum levels in patients with rheumatoid arthritis. *Mol Med* 13:210–215.

20. Borovikova LV, et al. (2000) Vagus nerve stimulation attenuates the systemic inflammatory response to endotoxin. *Nature* 405:458–462.

21. Tracey KJ (2007) Physiology and immunology of the cholinergic antiinflammatory pathway. *J Clin Invest* 117:289–296.

22. Evrengül H, et al. (2004) Heart rate variability in patients with rheumatoid arthritis. *Rheumatol Int* 24:198–202.

23. Bouton CE, et al. (2016) Restoring cortical control of functional movement in a human with quadriplegia. *Nature* 533:247–250.

24. Zanos TP, Mineault PJ, Pack CC (2011) Removal of spurious correlations between spikes and local field potentials. *J Neurophysiol* 105:474–486.

25. Zanos TP, Mineault PJ, Nasiotis KT, Guitton D, Pack CC (2015) A sensorimotor role for traveling waves in primate visual cortex. *Neuron* 85:615–627.

26. Zanos TP, Mineault PJ, Guitton D, Pack CC (2016) Mechanisms of saccadic suppression in primate cortical area V4. *J Neurosci* 36:9227–9239.

27. Steinberg BE, et al. (2016) Cytokine-specific neurograms in the sensory vagus nerve. *Bioelectron Med* 3:7–17.

28. Bourien J, et al. (2014) Contribution of auditory nerve fibers to compound action potential of the auditory nerve. *J Neurophysiol* 112:1025–1039.

29. Koh RG, Nachman AI, Zariffa J (2017) Use of spatiotemporal templates for pathway discrimination in peripheral nerve recordings: A simulation study. *J Neural Eng* 14: 016013.

30. Yoo PB, Durand DM (2005) Selective recording of the canine hypoglossal nerve using a multicontact flat interface nerve electrode. *IEEE Trans Biomed Eng* 52:1461–1469.

31. Binshtok AM, et al. (2008) Nociceptors are interleukin-1beta sensors. *J Neurosci* 28: 14062–14073.

32. Copray JCVM, et al. (2001) Expression of interleukin-1 beta in rat dorsal root ganglia. *J Neuroimmunol* 118:203–211.

33. Miller RJ, Jung H, Bhangoo SK, White FA (2009) Cytokine and chemokine regulation of sensory neuron function. *Handb Exp Pharmacol* 417–449.

34. Sorkin LS, Xiao W-H, Wagner R, Myers RR (1997) Tumour necrosis factor-α induces ectopic activity in nociceptive primary afferent fibres. *Neuroscience* 81:255–262.

35. Jin X, Gereau RW, 4th (2006) Acute p38-mediated modulation of tetrodotoxin-resistant sodium channels in mouse sensory neurons by tumor necrosis factor-α. *J Neurosci* 26:246–255.

36. Gudes S, et al. (2015) The role of slow and persistent TTX-resistant sodium currents in acute tumor necrosis factor-α-mediated increase in nociceptors excitability. *J Neurophysiol* 113:601–619.

37. Caterina MJ, et al. (2000) Impaired nociception and pain sensation in mice lacking the capsaicin receptor. *Science* 288:306–313.

38. Iida T, Shimizu I, Nealen ML, Campbell A, Caterina M (2005) Attenuated fever response in mice lacking TRPV1. *Neurosci Lett* 378:28–33.

39. De Winter BY, et al. (2009) Involvement of afferent neurons in the pathogenesis of endotoxin-induced ileus in mice: Role of CGRP and TRPV1 receptors. *Eur J Pharmacol* 615:177–184.

40. Musumeci G, et al. (2011) Transient receptor potential vanilloid 1 channels modulate the synaptic effects of TNF-α and of IL-1β in experimental autoimmune encephalomyelitis. *Neurobiol Dis* 43:669–677.

41. Meng J, Wang J, Steinhoff M, Dolly JO (2016) TNFα induces co-trafficking of TRPV1/TRPA1 in VAMP1-containing vesicles to the plasmalemma via Munc18-1/syntaxin1/SNAP-25 mediated fusion. *Sci Rep* 6:21226.

42. Story GM, et al. (2003) ANKTM1, a TRP-like channel expressed in nociceptive neurons, is activated by cold temperatures. *Cell* 112:819–829.

43. Caterina MJ, et al. (1997) The capsaicin receptor: A heat-activated ion channel in the pain pathway. *Nature* 389:816–824.

44. Caterina MJ, Julius D (2001) The vanilloid receptor: A molecular gateway to the pain pathway. *Annu Rev Neurosci* 24:487–517.

45. Peles S, et al. (2009) Differential effects of TRPV1 antagonists in acid-induced excitation of esophageal vagal afferent fibers of rats. *Neuroscience* 161:515–525.

46. Szallasi A, et al. (1995) Vanilloid (capsaicin) receptors in the rat: Distribution in the brain, regional differences in the spinal cord, axonal transport to the periphery, and depletion by systemic vanilloid treatment. *Brain Res* 703:175–183.

47. Üçeyler N, Schäfers M, Sommer C (2009) Mode of action of cytokines on nociceptive neurons. *Exp Brain Res* 196:67–78.

48. Liu L, Yang TM, Liedtke W, Simon SA (2006) Chronic IL-1beta signaling potentiates voltage-dependent sodium currents in trigeminal nociceptive neurons. *J Neurophysiol* 95:1478–1490.

49. Obreja O, Rathee PK, Lips KS, Distler C, Kress M (2002) IL-1 beta potentiates heat-activated currents in rat sensory neurons: Involvement of IL-1RI, tyrosine kinase, and protein kinase C. *FASEB J* 16:1497–1503.

50. Hou L, Li W, Wang X (2003) Mechanism of interleukin-1 beta-induced calcitonin gene-related peptide production from dorsal root ganglion neurons of neonatal rats. *J Neurosci Res* 73:188–197.

51. Goehler LE, Gaykema RP, Hammack SE, Maier SF, Watkins LR (1998) Interleukin-1 induces c-Fos immunoreactivity in primary afferent neurons of the vagus nerve. *Brain Res* 804:306–310.

52. Szallasi A, Blumberg PM (1999) Vanilloid (Capsaicin) receptors and mechanisms. *Pharmacol Rev* 51:159–212.

53. Zygmunt PM, et al. (1999) Vanilloid receptors on sensory nerves mediate the vasodilator action of anandamide. *Nature* 400:452–457.

54. Hermes SM, Andresen MC, Aicher SA (2016) Localization of TRPV1 and P2X3 in unmyelinated and myelinated vagal afferents in the rat. *J Chem Neuroanat* 72:1–7.

55. Helliwell RJ, et al. (1998) Capsaicin sensitivity is associated with the expression of the vanilloid (capsaicin) receptor (VR1) mRNA in adult rat sensory ganglia. *Neurosci Lett* 250:177–180.

56. del Valle J, Navarro X (2013) Interfaces with the peripheral nerve for the control of neuroprostheses. *Int Rev Neurobiol* 109:63–83.

57. Waters RL, McNeal DR, Faloon W, Clifford B (1985) Functional electrical stimulation of the peroneal nerve for hemiplegia. Long-term clinical follow-up. *J Bone Joint Surg Am* 67:792–793.

58. Tan DW, et al. (2014) A neural interface provides long-term stable natural touch perception. *Sci Transl Med* 6:257ra138.

59. Li C, et al. (2017) A new 3D self-adaptive nerve electrode for high density peripheral nerve stimulation and recording. *Proceedings of the Nineteenth IEEE International Conference on Solid-State Sensors, Actuators and Microsystems* (IEEE, Piscataway, NJ), pp 51–54.

60. Caravaca AS, et al. (2017) A novel flexible cuff-like microelectrode for dual purpose, acute and chronic electrical interfacing with the mouse cervical vagus nerve. *J Neural Eng* 14:066005.

61. Schuettler M, Donaldson N, Seetohul V, Taylor J (2013) Fibre-selective recording from the peripheral nerves of frogs using a multi-electrode cuff. *J Neural Eng* 10:036016.

62. Zariffa J, et al. (2011) A framework for the discrimination of neural pathways using multi-contact nerve cuff electrodes. *Conf Proc IEEE Eng Med Biol Soc* 2011:4645–4648.

63. Horn CC, Friedman MI (2003) Detection of single unit activity from the rat vagus using cluster analysis of principal components. *J Neurosci Methods* 122:141–147.

64. Zariffa J (2014) A review of source separation and source localization approaches in peripheral nerves. *Proceedings of the Forty-Eighth IEEE Asilomar Conference on Signals, Systems and Computers* (IEEE, Piscataway, NJ), pp 293–298.

65. Berthoud H-R, Neuhuber WL (2000) Functional and chemical anatomy of the afferent vagal system. *Auton Neurosci* 85:1–17.

66. Coleridge HM, Coleridge JCG (2011) Reflexes evoked from tracheobronchial tree and lungs. *Comprehensive Physiology* (John Wiley & Sons, Inc., Hoboken, NJ).

67. Chang RB, Strochlic DE, Williams EK, Umans BD, Liberles SD (2015) Vagal sensory neuron subtypes that differentially control breathing. *Cell* 161:622–633.

68. Kollarik M, Ru F, Brozmanova M (2010) Vagal afferent nerves with the properties of nociceptors. *Auton Neurosci* 153:12–20.

69. Yang NJ, Chiu IM (2017) Bacterial signaling to the nervous system through toxins and metabolites. *J Mol Biol* 429:587–605.

70. Cryan JF, Dinan TG (2012) Mind-altering microorganisms: The impact of the gut microbiota on brain and behaviour. *Nat Rev Neurosci* 13:701–712.

71. Silverman HA, et al. (2018) Standardization of methods to record Vagus nerve activity in mice. *Bioelectron Med* 4:3.

72. Eckberg DL, Nerhed C, Wallin BG (1985) Respiratory modulation of muscle sympathetic and vagal cardiac outflow in man. *J Physiol* 365:181–196.

73. Scharf LL (1991) *Statistical Signal Processing: Detection, Estimation, and Time Series Analysis* (Addison-Wesley, Reading, MA). Available at https://infoscience.epfl.ch/record/25888. Accessed September 19, 2017.

74. van der Maaten L, Hinton G (2008) Visualizing data using t-SNE. *J Mach Learn Res* 9: 2579–2605.

75. Gisbrecht A, Hammer B (2015) Data visualization by nonlinear dimensionality reduction. *Wiley Interdiscip Rev Data Min Knowl Discov* 5:51–73.

76. Ester M, Kriegel H-P, Sander J, Xu X (1996) A density-based algorithm for discovering clusters a density-based algorithm for discovering clusters in large spatial databases with noise. *Proceedings of the Second International Conference on Knowledge Discovery and Data Mining*, KDD'96. (Association for the Advancement of Artificail Intelligence, Portland, OR), pp 226–231.